Hybrid membrane-external-cavity surface-emitting laser

MINGYANG ZHANG,[1] ALEXANDER R. ALBRECHT,[1] CATHERINE NGUYEN,[2] DAVID FOLLMAN,[2] GARRETT D. COLE,[2] AND MANSOOR SHEIK-BAHAE[1,*]

[1]*Department of Physics and Astronomy, University of New Mexico, Albuquerque, NM 87131, USA*
[2]*Thorlabs Crystalline Solutions, Santa Barbara, CA 93101, USA*
*msb@unm.edu

Abstract: We develop, analyze, and demonstrate an optically-pumped semiconductor disk laser using an active mirror architecture formed by sandwiching the semiconductor gain membrane between two heatspreaders, one of which is coated with a high-reflectivity multilayer. Thermal modeling indicates that this structure outperforms traditional VECSELs. Employing an InGaAs/GaAs MQW gain structure, we demonstrate output powers of approximately 30 W at a center wavelength of $\lambda \approx 1178$ nm in a TEM_{00} mode using an in-well pumped geometry.

1. Introduction

Enormous progress in research and applications of optically-pumped semiconductor disk lasers (OPSLs, SDLs), also known as vertical-external-cavity surface-emitting lasers (VECSELs), has been made in the last two and a half decades [1–6]. As depicted in Fig. 1(a), the most common architecture employs a gain module that operates as an active mirror, formed by the gain medium (typically multiple quantum wells, MQW) that is epitaxially grown on top of a distributed Bragg reflector (DBR) [1,3]. This gain assembly is then soldered to a heatspreader (commonly CVD diamond), which is placed in thermal contact with the heat sink (often water-cooled copper blocks), with the laser cavity enclosed by an external mirror acting as the output coupler. A typical VECSEL in a linear cavity configuration is shown in Fig. 1(b). As an alternative to this layout, a DBR-free gain-chip architecture, also known as a membrane-external-cavity surface-emitting laser (MECSEL), was later introduced. This structure offers excellent flexibility over traditional VECSELs, while providing superior thermal management [7–11].

The MECSEL gain module, as shown in Fig. 1(c), consists of the semiconductor gain material only (lacking an integrated DBR) direct-bonded to one—or sandwiched between two—heatspreader(s) (such as SiC, diamond, or sapphire). Like most solid-state lasers, the laser cavity can therefore be formed by fully external (typically dielectric) mirrors. An example of a MECSEL gain module, again in a linear two mirror standing-wave cavity, is shown in Fig. 1(d).

Most (if not nearly all) SDLs, including VECSELs, employ an MQW active region, with each quantum well positioned at an antinode of the standing wave, which has a cavity node pinned at the surface of the integrated DBR. This is known as the resonant periodic gain (RPG) architecture [12] though nonresonant (non-RPG) configurations have also been investigated to achieve broadband tunability or modelocking operation [13]. It was shown that the RPG structure in MECSELs, together with broadband dielectric mirrors, can potentially provide a two-fold larger wavelength tunability than RPG-VECSELs [14], with potential for modelocked operation in the future [15].
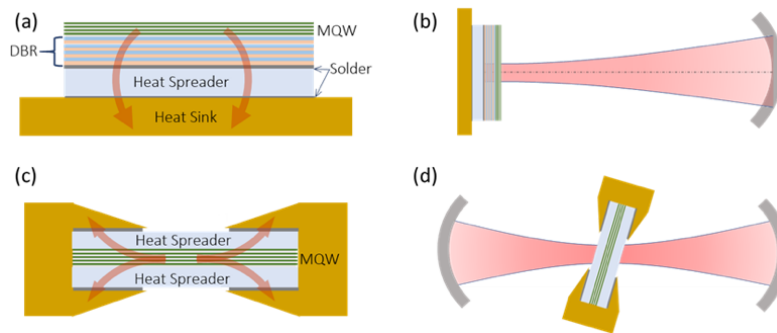
Fig. 1. Comparison of traditional VECSEL and MECSEL architectures. (a) Cross-sectional schematic of a standard VECSEL gain chip with a MQW active region monolithically integrated with a DBR. (b) Linear cavity configuration for a typical VECSEL structure. (c) Schematic of a MECSEL gain chip with the MQW gain material sandwiched between two direct-bonded heatspreaders. (d) In this device the optical resonator is fully external. In panels (a) and (c) the arrows (in red) indicate the direction of heat flux.

2. Hybrid MECSEL

In this paper, we introduce a modified (hybrid) MECSEL architecture, which we dub the "H-MECSEL", that uses a mirrored heatspreader. In this device the laser configuration is thus similar to a traditional VECSEL; however, in this case, the MQW active region is directly contacted to the heatspreaders with an external integrated mirror. A schematic of such a gain module is shown in Fig. 2(a) for the case of a double heatspreader structure. The mirror on the heatspreader can
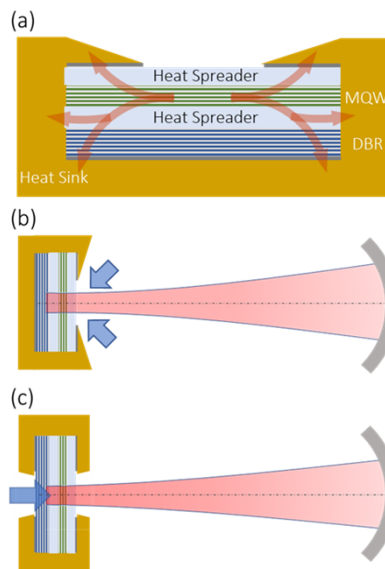

Fig. 2. Examples of double-heat-spreader H-MECSEL systems: (a) the gain module, where red arrows show the approximate heat-flux pathways, (b) & (c) simple H-MECSEL laser cavity with front and backside pumping schemes, respectively. The back mirror in (c) exhibits high reflectivity (HR) at the laser wavelength and high transmission (HT) for the pump.

be a standard optical interference coating (such as a dielectric multilayer), as well as a crystalline DBR (e.g., epitaxially grown semiconductor structure that is directly bonded to the heatspreader [16,17]). Alternatively, metallic reflectors or hybrid combinations of semiconductors, dielectrics, and/or metals can be employed in order to optimize the thermal and optical performance of the mirror. Such a structure offers multiple advantages in terms of the simplification of the pumping scheme, ease of cavity design, and compactness (as diagrammatically illustrated in Fig. 2), while retaining or even improving the heat dissipation of the MECSEL, as will be described next.
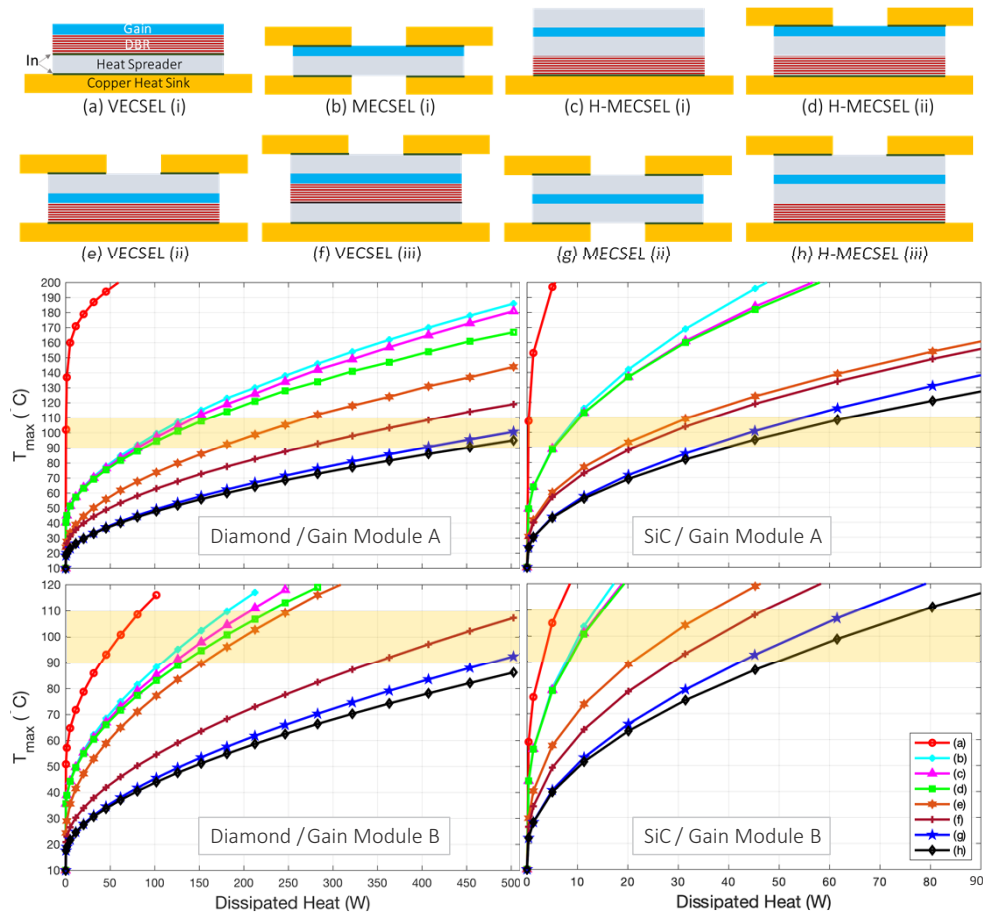

Fig. 3. The maximum on-axis temperature versus total dissipated heat power for the various VECSEL, MECSEL, and H-MECSEL geometries shown on top: a, e, and f are VECSELs with bottom, intra-cavity, or dual heat spreaders; b and g are MECSELs with one and two heat spreaders; d is an H-MECSEL with one heat spreader, c and h are dual heat spreader H-MECSELs connected to one or two heatsinks. A Gaussian heat source with constant heat intensity (40 kW/cm^2) with varying spot size is assumed. The data shown are for diamond (left) and SiC (right) heatspreaders. The top and bottom panels correspond to gain modules (A) and (B) respectively, assuming different gain and DBR thicknesses, as well as the thermal conductivities as specified in Table 1. The shaded temperature range (90 $^\circ C < T_{max} < 110\,^\circ C$) indicates the region where thermal rollover is expected to occur.

Table 1. Thermal properties and thicknesses of the materials used in the thermal analysis for various gain modules described in Fig. 3

κ_{InGaP}	Thermal Conductivity of Window Layer	10 W/(m · K)
κ_{gain}	Thermal Conductivity of Active Region	35 W/(m · K) [A] 24 W/(m · K) [B]
κ_{DBR}	Thermal Conductivity of DBR	25 W/(m · K) [A] 61 W/(m · K) [B]
κ_{In}	Thermal Conductivity of Indium	84 W/(m · K)
κ_{SiC}	Thermal Conductivity of 4H-SiC	390 W/(m · K)
$\kappa_{diamond}$	Thermal Conductivity of Diamond	1800 W/(m · K)
κ_{copper}	Thermal Conductivity of Copper Mount	400 W/(m · K)
d_{InGaP}	Thickness of Window Layer	214 nm
d_{gain}	Thickness of Active Region	3.56 μm [A] 2.25 μm [B]
d_{DBR}	Thickness of dual-band DBR	9.07 μm [A] 3.72 μm [B]
d_{In}	Thickness of Indium	20 μm
d_{SiC}	Thickness of SiC	500 μm
$d_{diamond}$	Thickness of Diamond	500 μm
$\left. \dfrac{dn}{dT} \right\|_{SiC}$	Thermo-Optic Coefficient of 4H-SiC	3.5×10^{-5} 1/K
$\left. \dfrac{dn}{dT} \right\|_{diamond}$	Thermo-Optic Coefficient of Diamond	9.6×10^{-6} 1/K

3. Thermal analysis

Using COMSOL finite element modeling software, we performed a detailed thermal transport analysis in order to compare H-MECSEL gain modules with MECSELs and traditional VECSELs [7,18]. Various MECSEL and H-MECSEL configurations such as single or double heatspreaders, as well as single or double heatsinks, were considered in these efforts. The results are summarized in Fig. 3, where the calculated maximum (on-axis) temperature is displayed as a function of heat power deposited assuming a Gaussian heat source that follows the pump laser profile $P_{heat}(r) = P_0 e^{-2r^2/w_p^2}$. It is evident that the H-MECSEL outperforms not only traditional VECSELs, but also exhibits moderate improvement over its MECSEL counterpart, while offering flexibility in pumping and cavity designs, as stated earlier. The shaded area in Fig. 3 corresponding to $90\,°C < T_{max} < 110\,°C$, is typically considered the temperature range associated with the onset of thermal rollover in semiconductor disk lasers [19,20]. The material parameters used in this simulation are listed in Table 1. Here we consider two types of gain modules in our thermal model. Module (A) pertains to the system studied experimentally in this paper involving a thick ($\sim 10\,\mu$m) dual-band DBR and thick ($\sim 3.5\,\mu$m, corresponding to 20 QWs) active region (for in-well pumping) with their corresponding thermal conductivities. Module (B) assumes a thinner thermally optimized single-wavelength DBR, as well as a thinner gain medium which are more typical of the standard diode-pumped SDL. For consistency with the earlier simulations for module (B), we used the relatively high thermal conductivity for the DBR (~ 60 W/mK), which is somewhat of an overestimate when compared to an all semiconductor mirror, but can be realized with a hybrid semiconductor/metal structure [7,21].

Thermal Lensing: The use of intracavity heatspreaders, whether in VECSELs or MECSELs, while alleviating the thermal loading on the gain chip, may introduce undesirable thermal lensing. This is important in MECSEL and H-MECSEL structures and thus should be addressed, minimized, and taken into consideration in designing the requisite laser cavity. Having calculated the radial temperature profile in the COMSOL thermal analysis, an effective thermal focal length can be obtained by the well-known parabolic approximation of this radial profile [22,23]. In MECSELs and H-MECSELs, this lensing is dominated by the thermo-optic effects in the

heatspreaders, with known coefficients of dn/dT and thermal conductivity (κ). The lensing in the thin semiconductor gain layer and the effects of thermal expansion can be ignored. A typical temperature profile in an H-MECSEL is shown in Fig. 4(a) with a parabolic fit to the average (along with the z-direction) radial temperature profile assuming double 4H-SiC heatspreaders (see Table 1 for properties). Under such approximations, and assuming cylindrically symmetric excitation and boundary conditions for solid-state lasers, the thermal lens power ($1/f_{th}$) has been shown to follow $\frac{P_{heat}}{\pi w_p^2} \left[\frac{1}{\kappa} \frac{dn}{dT} \right]$ [24]. We find that a more rigorous thermal analysis for the MECSEL and H-MECSEL geometries shown in Fig. 3, leads to an effective lens power that can be approximated by:

$$\frac{1}{f_{th}} \approx K \frac{P_{heat}}{w_p^\beta}, \tag{1}$$

where $\beta = 1.4$, $K = 5.7 \times 10^{-7}$ and 2.9×10^{-8} (SI units), for SiC and diamond heatspreaders, respectively. The simulated values of the thermal lens power versus the dissipated power along with the linear fits using Eq. (1) for both SiC and diamond heat-spreaders are shown in Fig. 4(b). As with other thin-disk lasers under high power operation, thermal lensing can be mitigated using larger mode areas in the active region. Alternatively, though more costly in high optical quality grades, diamond heatspreaders result in negligible thermal lensing, smaller than SiC by more than an order of magnitude.
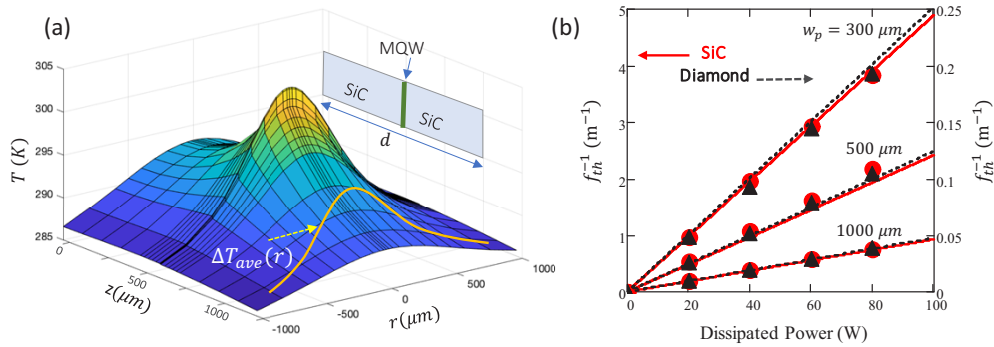

Fig. 4. (a) A typical 3D temperature profile calculated for a double SiC H-MECSEL using the parameters in Table 1 (gain module B). The temperature profile $\Delta T_{ave}(r)$, averaged over the total length of the heatspreaders is used to calculate the thermal lens focal length. (b) The calculated power of the induced thermal lens in a double heatspreader configuration versus the total dissipated heat power for SiC (left axis) and diamond (right axis) for various Gaussian pump spot sizes. The lines (solid for SiC, dashed for diamond) are the linear fits using Eq. (1).

4. Experimental demonstration of an in-well pumped H-MECSEL

With the simulations completed, Fig. 5 shows a schematic of the H-MECSEL device experimentally investigated in this effort. The MQW structure is deposited via metal organic chemical vapor deposition (MOCVD) on GaAs substrates (gain material supplied by Twenty-One Semiconductors GmbH, Stuttgart, Germany). The structural design of the gain medium is similar to that reported in [25,26]. The 20 quantum-well (QW) structure comprises InGaAs QWs and GaAs barriers arranged in an RPG design for maximum enhancement. InGaP window layers prevent carrier recombination and protect the active region during substrate removal. The active region is direct bonded (without the use of adhesives, solders, or interlayers) between two 4H-SiC heatspreaders, each 500 μm thick, using an extension of the substrate transfer coating process described in

[15,16]. We realize nearly 100% yield in production, particularly when using SiC heatspreaders that benefit from extremely high surface quality and material availability at standard wafer sizes. Recently, we have demonstrated the simultaneous production of hundreds of such gain elements in a wafer-scale batch fabrication process when employing 4" (10 cm) diameter MQW epi wafers and SiC heatspreader wafers [27]. Our approach leverages low-temperature plasma-activated bonding in concert with traditional microfabrication steps (dielectric and metal deposition, lithography, chemical, and plasma etching, etc.), allowing hundreds of devices to be simultaneously produced.
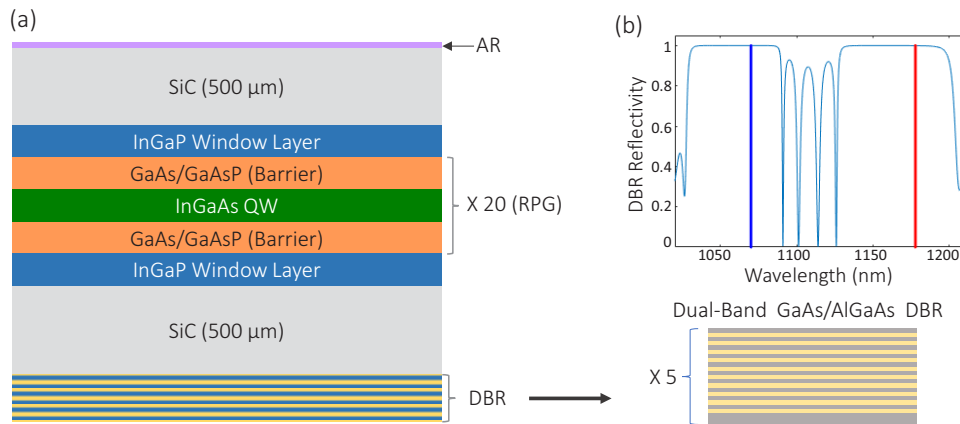

Fig. 5. (a) Schematic of the H-MECSEL gain module comprising MOCVD-grown strain-compensated InGaAs-GaAs QWs (×20) in an RPG arrangement. The active region is bonded between two SiC substrates. The front SiC heatspreader is AR coated at the pump wavelength (1070 nm), while the backside SiC heatspreader includes an epitaxial dual-band DBR (HR @ 1178 nm and 1070 nm) using our direct-bonding-based substrate-transfer coating process. (b) The bottom schematic shows the structure of the dual-band DBR consisting of 5 stacks, each containing 10 quarter-wave pairs of high-index (GaAs)/ low-index (AlGaAs) layers, with each stack separated by a thick high index (GaAs) layer. The top plot shows the calculated reflectance of the DBR

Following the MECSEL chip production process, an AR coating (at the pump wavelength only) is deposited on the front surface of one of the SiC heatspreaders. In order to generate the H-MECSEL, we directly bond a dual-band GaAs/AlGaAs DBR to the second heatspreader. The dual-band DBR is based on the design from C.P. Lee, et al., comprising the addition of two periodic functions [28]. This multi-periodic structure, with appropriate phase shifters, enables HR functionality at both wavelengths of interest for the laser, including 1178 nm for the fundamental emission and 1070 nm for the in-well pump. This structure was grown by molecular beam epitaxy (MBE), owing to its low background impurity level and thus low optical absorption [16,17]. Transferred to the SiC and with a Ti/Au backing, the mirror exhibits a reflectance of 99.997% at 1070 nm and 99.93% at 1178 nm. Following the heatspreader and back mirror bonding processes (+ AR coating), the completed gain element is mounted in a water-cooled copper heat-sink with In foil, similar to the schematic shown in Fig. 2(a).

As was demonstrated in our previous work with a standard MECSEL gain structure using the same active material and heatspreaders [25], in-well pumping leads to a reduced quantum defect, allowing us to operate this laser at higher powers. Analogous to the MECSEL arrangement of [25], a multi-pass pump circulator is designed and assembled, but this time in a simplified reflection geometry as shown in Fig. 6. The setup consists of a pair of flat high-reflectivity mirrors forming a retroreflector at the pump wavelength. The mirror axis is displaced to introduce a slight lateral shift of the pump beam upon each retroreflection. An aspheric lens (f_a=10 cm,

D=5.08 cm) is positioned roughly 10 cm from the gain chip and mirror pair with a central hole for passing the laser light.
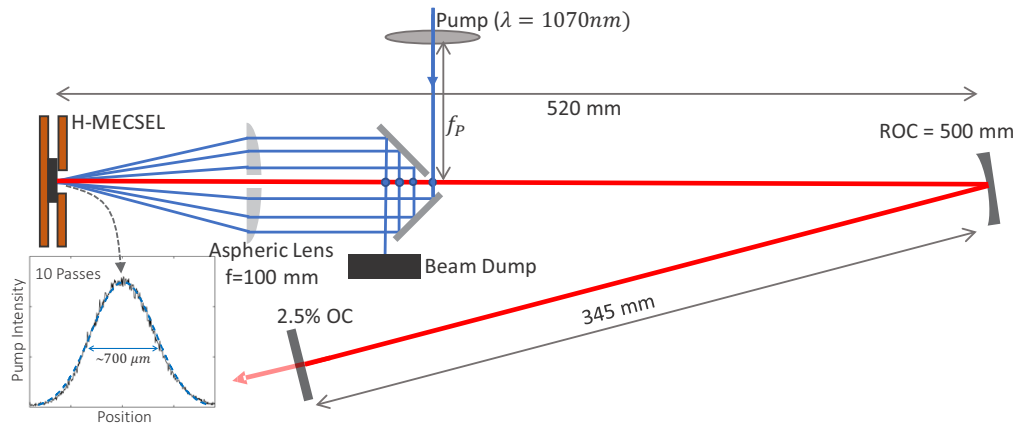

Fig. 6. Schematic of the laser cavity used in the experimental demonstration of the H-MECSEL. The cavity is formed by the gain chip with backside DBR, a concave HR mirror, and a flat output coupler. Multipass in-well pumping is achieved using a combination of flat folding mirrors and an aspheric lens. The inset shows the measured beam profile after 10 passes of the pump laser. The cavity laser mode is directed through a small hole drilled in the center of the aspheric lens.

The H-MECSEL resonator is constructed in a V-cavity geometry formed by the H-MECSEL gain chip, a concave mirror with ROC=50 cm (tilted at an angle of 8°), and a flat output coupler (OC) having a transmission of 2.5%. The cavity schematic and its dimensions are shown in Fig. 6. The pump laser is a high-power (up to 500 W) unpolarized CW Yb-fiber laser (IPG Photonics) at 1070 nm. Using a combination of a half-wave plate and polarizing cubes, we obtain variable power up to 210 W with linear polarization for in-well pumping.

The pump beam is focused using a lens having a focal length f_p =75 cm at a distance of 10 cm (=f_a) from the aspheric lens which collimates the beam before illuminating the gain medium. The pump beam is then reflected by the DBR on the back of the H-MECSEL gain chip and re-focused by the aspheric lens. This process will repeat multiple times before the beam exits the circulator onto a beam dump. The plot in Fig. 6 illustrates the intensity profile of the pump beam resulting from ten passes (or 5 roundtrips) in the circulator plotted along with a Gaussian fit having FWHM diameter of ~700 μm ($w_p \approx 590$ μm). The cavity mode is directed through a 3 mm diameter hole drilled in the center of the aspheric lens; it has a FWHM diameter of ~415 μm on the gain chip, calculated assuming a thermal lens focal length of $f_{th} = 1$ m obtained from Eq. (1) at an estimated dissipated (thermal loading) power of 50 W.

The measured free-running output power of the H-MECSEL versus the absorbed pump power is shown in Fig. 7. The absorbed power (~41% of incident power) is estimated from the difference between the incident and the reflected pump power from the gain chip and the multipass pumping optics.

We demonstrate up to 28 W of output at $\lambda = 1178$ nm at a slope efficiency of ~38% (threshold of ~10 W) with no noticeable rollover at the highest absorbed power of 86 W (corresponding to ~210 W incident). From the thermal simulation of Fig. 3, and assuming a thermal loading of 50 W, a maximum temperature of ~100 °C is estimated in the active region, which might be approaching roll-over, though our thermal model is likely conservative and overestimating the active region temperature. The spectrum and the beam profile at the maximum output are shown in the upper left inset and lower right inset of Fig. 7, respectively. The mode spacing in the
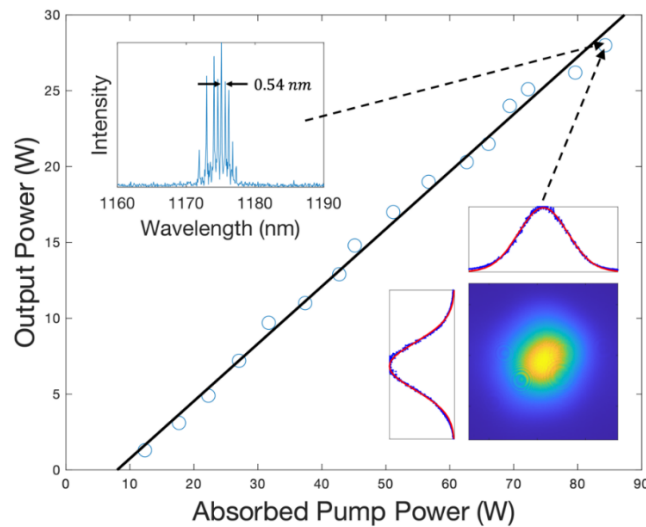
Fig. 7. Measured output power of the CW H-MECSEL versus the absorbed pump power (at λ =1070 nm). The free-running output spectrum (upper-left inset), and the beam profile (lower-right inset) are measured at the maximum output power of ~28 W.

spectrum corresponds to 0.54 nm, which is the free-spectral-range of the subcavity formed by the top SiC heatspreader. Such multimode oscillation under free running operation is expected due to some small degree of inhomogeneous broadening that is present in MQW gain media. The output beam profile, measured using a commercial beam profiler at a distance of ~50 cm away from the output coupler, exhibits a single-mode (TEM$_{00}$) structure as can be seen in the lower right inset in the same figure. In comparison with our previous work using ordinary MECSEL based on the same gain chip (having a slope efficiency of ~28%) [25], the H-MECSEL platform offers various advantages including a simpler and potentially shorter cavity design, more convenient pumping arrangement (particularly in multipass in-well pumping geometry) and higher slope efficiency.

It should also be noted that this gain structure, having 20 QWs, was specifically designed for in-well pumping by allowing sufficient pump absorption per pass, thus maximizing the efficiency of our multipass pumping scheme. Nonetheless, for comparison we also performed barrier pumping tests using 808 nm diode lasers. Since most of the pump power is absorbed near the top QWs, leading to a nonuniform distribution of carriers and gain/loss, this resulted in sub-optimum performance. For example, with 50 W incident power at 808 nm, an output power of ~6 W was measured, along with a slope efficiency of 12%.

5. Conclusions

We have introduced the concept and experimentally demonstrated a novel hybrid MECSEL, integrating a high-reflectivity mirror on the backside of an intracavity heatspreader, operating at a center wavelength of 1178 nm. The gain structure consists of 20 InGaAs/GaAs MQWs sandwiched between two SiC heatspreaders, with a dual-band semiconductor (GaAs/AlGaAs) DBR transferred to one of the SiC heatspreaders. Employing a multipass in-well pumping scheme, this so-called H-MECSEL exhibits a maximum CW power of 28 W at an absorbed power of 80 W from a pump laser at 1070 nm without any thermal rollover. Our detailed thermal analysis also indicates that the H-MECSEL platform outperforms standard VECSELs and MECSELs. Finally, we addressed the thermal lensing in such lasers and presented a simple empirical expression for estimating thermal lens power for SiC and diamond heatspreaders.

Disclosures. The authors declare no conflicts of interest.

Data availability. Data underlying the results presented in this paper are not publicly available at this time but may be obtained from the authors upon reasonable request.

References

1. M. Kuznetsov, F. Hakimi, R. Sprague, and A. Mooradian, "High-power (>0.5-W CW) diode-pumped vertical-external-cavity surface-emitting semiconductor lasers with circular TEM00 beams," IEEE Photonics Technol. Lett. **9**(8), 1063–1065 (1997).
2. M. Guina, A. Rantamäki, and A. Härkönen, "Optically pumped VECSELs: Review of technology and progress," J. Phys. D: Appl. Phys. 50(38), 383001 (2017).
3. O. G. Okhotnikov, "Semiconductor Disk Lasers: Physics and Technology," Wiley-VCH, 2010.
4. M. Jetter and P. Michler, "Vertical External Cavity Surface Emitting Lasers: VECSEL Technology and Applications," Wiley-VCH, 2021.
5. B. Heinen, T.-L. Wang, M. Sparenberg, A. Weber, B. Kunert, J. Hader, S. W. Koch, J. V. Moloney, M. Koch, and W. Stolz, "106 W continuous-wave output power from vertical-external-cavity surface-emitting laser," Electron. Lett. **48**(9), 516 (2012).
6. A. Rahimi-Iman, "Recent advances in VECSELs," J. Opt. **18**(9), 093003 (2016).
7. Z. Yang, A. R. Albrecht, J. G. Cederberg, and M. Sheik-Bahae, "Optically pumped DBR-free semiconductor disk lasers," Opt. Express **23**(26), 33164 (2015).
8. H. Kahle, C. M. N. Mateo, U. Brauch, P. Tatar-Mathes, R. Bek, M. Jetter, T. Graf, and P. Michler, "Semiconductor membrane external-cavity surface-emitting laser (MECSEL)," Optica **3**(12), 1506–1512 (2016).
9. S. Mirkhanov, A. H. Quarterman, H. Kahle, R. Bek, R. Pecoroni, C. J. C. Smyth, S. Vollmer, S. Swift, P. Michler, M. Jetter, and K. G. Wilcox, "DBR-free semiconductor disc laser on SiC heatspreader emitting 10.1 W at 1007 nm," Electron. Lett. **53**(23), 1537–1539 (2017).
10. Z. Yang, D. Follman, A. R. Albrecht, P. Heu, N. Giannini, G. D. Cole, and M. Sheik-Bahae, "16 W DBR-free membrane semiconductor disk laser with dual-SiC heatspreader," Electron. Lett. **54**(7), 430–432 (2018).
11. A. R. Albrecht, Z. Yang, and M. Sheik-Bahae, "DBR-free Optically Pumped Semiconductor Disk Lasers," in *Vertical External Cavity Surface Emitting Lasers*, M. Jetter and P. Michler, eds. (Wiley-VCH, 2021), pp. 175–196.
12. M. Y. A. Raja, S. R. J. Brueck, M. Osinski, C. F. Schaus, J. G. McInerney, T. M. Brennan, and B. E. Hammons, "Resonant Periodic Gain Surface-Emitting Semiconductor Lasers," IEEE J. Quantum Electron. **25**(6), 1500–1512 (1989).
13. A. Laurain, I. Kilen, J. Hader, A. Ruiz Perez, P. Ludewig, W. Stolz, S. Addamane, G. Balakrishnan, S. W. Koch, and J. V. Moloney, "Modeling and experimental realization of modelocked VECSEL producing high power sub-100 fs pulses," Appl. Phys. Lett. **113**(12), 121113 (2018).
14. Z. Yang, A. R. Albrecht, J. G. Cederberg, and M. Sheik-Bahae, "80 nm tunable DBR-free semiconductor disk laser," Appl. Phys. Lett. **109**(2), 022101 (2016).
15. M. Sheik-Bahae, "Analysis of MECSEL mode-locking," Proc. SPIE **11984**, 1198405 (2022).
16. G. D. Cole, W. Zhang, M. J. Martin, J. Ye, and M. Aspelmeyer, "Tenfold reduction of Brownian noise in high-reflectivity optical coatings," Nat. Photonics **7**(8), 644–650 (2013).
17. G. D. Cole, W. Zhang, B. J. Bjork, D. Follman, P. Heu, C. Deutsch, L. Sonderhouse, J. Robinson, C. Franz, A. Alexandrovski, M. Notcutt, O. H. Heckl, J. Ye, and M. Aspelmeyer, "High-performance near- and mid-infrared crystalline coatings," Optica **3**(6), 647–656 (2016).
18. H.-M. Phung, P. Tatar-Mathes, A. Rogers, P. Rajala, S. Ranta, H. Kahle, and M. Guina, "Thermal Behavior and Power Scaling Potential of Membrane External-Cavity Surface-Emitting Lasers (MECSELs)," IEEE J. Quantum Electron. **58**(2), 1–11 (2022).
19. Y. Huo, C. Y. Cho, K. F. Huang, Y. F. Chen, and C. C. Lee, "Exploring the DBR superlattice effect on the thermal performance of a VECSEL with the finite element method," Opt. Lett. **44**(2), 327–330 (2019).
20. J. Hader, T. L. Wang, J. V. Moloney, B. Heinen, M. Koch, S. W. Koch, B. Kunert, and W. Stolz, "On the measurement of the thermal impedance in vertical-external-cavity surface-emitting lasers," J. Appl. Phys. **113**(15), 153102 (2013).
21. J. Piprek, T. Tröger, B. Schröter, J. Kolodzey, and C. S. Ih, "Thermal conductivity reduction in GaAs-AlAs distributed Bragg reflectors," IEEE Photonics Technol. Lett. **10**(1), 81–83 (1998).
22. W. Koechner, "Thermal Lensing in a Nd:YAG Laser Rod," Appl. Opt. **9**(11), 2548–2553 (1970).
23. L. M. Osterink and J. D. Foster, "Thermal effects and transverse mode control in a Nd:YAG laser," Appl. Phys. Lett. **12**(4), 128–131 (1968).

24. M. E. Innocenzi, H. T. Yura, C. L. Fincher, and R. A. Fields, "Thermal modeling of continuous-wave end-pumped solid-state lasers," Appl. Phys. Lett. **56**(19), 1831–1833 (1990).

25. D. Priante, M. Zhang, A. R. Albrecht, R. Bek, M. Zimmer, C. L. Nguyen, D. P. Follman, G. D. Cole, and M. Sheik-Bahae, "In-Well Pumping of a Membrane External-Cavity Surface-Emitting Laser," IEEE J. Sel. Top. Quantum Electron. **28**(1: Semiconductor Lasers), 1–7 (2022).

26. D. Priante, M. Zhang, A. R. Albrecht, R. Bek, M. Zimmer, C. Nguyen, D. Follman, G. D. Cole, and M. Sheik-Bahae, "Demonstration of a 20-W membrane-external-cavity surface-emitting laser for sodium guide star applications," Electron. Lett. **57**(8), 337–338 (2021).

27. G. D. Cole, C. Nguyen, D. Follman, R. Bek, M. Zimmer, N. Witz, M. Zhang, A. R. Albrecht, and M. Sheik-Bahae, "Chip- and Wafer-Scale Manufacturing of High-Power Membrane-External-Cavity Surface-Emitting Laser Gain Elements," in *Conference on Lasers and Electro-Optics (2022)*, Paper ATh2L.2 (Optica Publishing Group, 2022), p. ATh2L.2.

28. C. P. Lee, C. M. Tsai, and J. S. Tsang, "Dual-wavelength Bragg reflectors using GaAs/AlAs multilayers," Electron. Lett. **29**(22), 1980–1981 (1993).